Article

Mechanistic Insight into Concerted Proton-Electron Transfer of a Ru(IV)-Oxo Complex: A Possible Oxidative Asynchronicity

Hiroaki Kotani, hinatsu shimomura, Kei Ikeda, Tomoya Ishizuka, Yoshihito Shiota, Kazunari Yoshizawa, and Takahiko Kojima

J. Am. Chem. Soc., **Just Accepted Manuscript** • DOI: 10.1021/jacs.0c05738 • Publication Date (Web): 14 Sep 2020

Mechanistic Insight into Concerted Proton-Electron Transfer of a Ru(IV)-Oxo Complex: A Possible Oxidative Asynchronicity

Hiroaki Kotani,[†] Hinatsu Shimomura,[†] Kei Ikeda,[‡] Tomoya Ishizuka,[†] Yoshihito Shiota,[‡] Kazunari Yoshizawa[‡], and Takahiko Kojima[†,*]

[†] *Department of Chemistry, Faculty of Pure and Applied Sciences, University of Tsukuba and CREST (JST), 1-1-1 Tennoudai, Tsukuba, Ibaraki 305-8571, Japan*

[‡] *Institute for Materials Chemistry and Engineering, Kyushu University and CREST (JST), Motooka, Nishi-Ku, Fukuoka 819-0395, Japan*

ABSTRACT: We have thoroughly investigated oxidation of benzyl alcohol (BA) derivatives by a $Ru^{IV}(O)$ complex (**$Ru^{IV}(O)$**) in the absence or presence of Brønsted acids in order to elucidate the proton-coupled electron-transfer (PCET) mechanisms in C-H oxidation on the basis of kinetic analysis. Oxidation of BA derivatives by **$Ru^{IV}(O)$** without acids proceeded through concerted proton-electron transfer (CPET) with a large kinetic isotope effect (KIE). In contrast, oxidation of 3,4,5-trimethoxy-BA ($(MeO)_3$-BA) by **$Ru^{IV}(O)$** was accelerated by addition of acids, in which the KIE value was reached to 1.1 with TFA (550 mM), indicating an alteration of the PCET mechanism from CPET to stepwise electron transfer (ET) followed by proton transfer (PT). Although the oxidized products of BA derivatives were confirmed to be the corresponding benzaldehydes in the range of acid concentrations (0 – 550 mM), a one-electron reduction potential of **$Ru^{IV}(O)$** was positively shifted with increasing the concentrations of acids. The elevated reduction potential of **$Ru^{IV}(O)$** strongly influenced the PCET mechanisms in oxidation of $(MeO)_3$-BA, changing the mechanism from CPET to ET/PT, as evidenced by driving-force dependence of logarithms of reaction rate constants in light of the Marcus theory of ET. In addition, dependence of activation parameters on acid concentrations suggested that an oxidative asynchronous CPET, which is not admixture of the CPET and ET/PT mechanisms, is probably operative in the boundary region (0 mM < [TFA] < 50 mM) involving a one-proton-interacted **$Ru^{IV}(O)\cdots H^+$** as a dominant reactive species.

INTRODUCTION

Hydrogen-atom transfer (HAT) from X-H bonds to high-valent metal-oxo complexes ($M^{n+}(O)$) is a fundamental step for oxidative transformation of organic substrates in both biological and artificial systems.[1-3] So far, HAT reactions from C-H bonds of organic substrates to $M^{n+}(O)$ have been extensively investigated to understand the controlling factors and mechanisms.[4,5] In the course of HAT reactions, $M^{n+}(O)$ is capable of accepting a net hydrogen atom ($H\bullet = e^- + H^+$) directly via proton-coupled electron transfer (PCET), in which an electron is accepted by the metal center and a proton by the oxo ligand, respectively.[6-8] As shown in Figure 1, PCET mechanisms in oxidation of substrates have been categorized into several pathways such as concerted proton-electron transfer (CPET), and stepwise pathways (electron transfer (ET) followed by proton transfer (PT), ET/PT, or PT followed by ET, PT/ET), depending on the characteristics of $M^{n+}(O)$ and substrates.[6b] Therefore, the scrutiny of controlling factors in PCET is indispensable for elucidating the reactivity of $M^{n+}(O)$ because CPET reactions are thermodynamically favorable as compared to stepwise ET/PT or PT/ET from substrates to $M^{n+}(O)$.

In order to investigate PCET from substrates to $M^{n+}(O)$, a borderline of PCET mechanisms should be clarified by changing the parameters of $M^{n+}(O)$ or substrates. For example, Fukuzumi and co-workers have reported acid-promoted substrate oxidation by Fe^{IV}-oxo complexes, in which the PCET mechanism is altered from CPET to stepwise ET/PT in the presence of acids by changing the one-electron reduction potential (E_{red}) of Fe^{IV}-oxo complexes.[9] Recently, Anderson and co-workers have demonstrated a basic

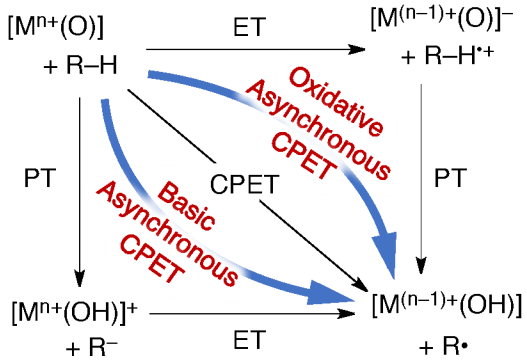

Figure 1. PCET mechanisms in oxidation of substrates (R–H) by metal-oxo complexes ($M^{n+}(O)$)

asynchronous CPET mechanism (Figure 1) in oxidation of C-H bonds by a Co^{III}-oxo complex, in which pK_a values of C-H bonds in substrates are determinants for the reaction kinetics of HAT.[10] As depicted in Figure 1, another pathway of asynchronous CPET is an oxidative asynchronous CPET, in which redox potentials of substrates or oxidants, which act as hydrogen-atom acceptors such as $M^{n+}(O)$, rather than those pK_a values are responsible for the HAT kinetics. The asynchronous CPET is defined as an intermediate pathway through a transition state bearing an ET or PT character between CPET and stepwise mechanisms (ET/PT or PT/ET) as shown in Figure 1.[10-13] As mentioned above, although a basic asynchronous CPET pathway has been demonstrated using the $Co^{III}(O)$

complex as well as other compounds,[11] an oxidative asynchronous CPET pathway has yet to be argued in detail. Judging from reported C-H oxidation by $M^{n+}(O)$, the PCET mechanisms depend on underlying characteristics of both $M^{n+}(O)$ and substrates, which include pK_a of the oxo ligand and a C-H bond of a substrate, their redox potentials (E) to determine a driving force of ET ($-\Delta G_{et}$) from a substrate to $M^{n+}(O)$ and especially reorganization energy (λ) of ET for $M^{n+}(O)$.[6,9,14,15] As reported previously, interaction of a proton with $M^{n+}(O)$ elevates the redox potential of $M^{n+}(O)$ to increase the driving force of ET from a substrate. Thus, it is expected that the interaction of a proton with $M^{n+}(O)$ should enhance the ET character in the transition state of a CPET process in C-H oxidation.

Among a series of $M^{n+}(O)$ complexes, high-valent Ru-oxo complexes have also been intensively investigated as active species in substrate oxidation reactions including C-H oxidation.[16-20] It has been revealed that C-H oxidation of cumene by $Ru^{IV}(O)$ complexes is initiated by hydrogen atom abstraction, followed by an oxygen-rebound process to afford cumyl alcohol in CH_3CN.[15b,20b] In the course of HAT from the C-H bond to a $Ru^{IV}(O)$ complex, the CPET pathway has been accepted in light of arguments based on the Bell-Evans-Polanyi principle;[4,5a] however, influence of protons on the asynchronicity of CPET from a C-H bond to a $Ru^{IV}(O)$ complex has yet to be scrutinized.

Here, we report mechanistic insights into oxidation reactions of benzyl alcohol (BA) derivatives by an isolated $Ru^{IV}(O)$ complex, $[Ru^{IV}(O)(MeBPA)(bpy)]^{2+}$ (**$Ru^{IV}(O)$**) (MeBPA = *N*-methyl-*N*,*N*-bis(2-pyridyl methyl)amine, bpy = 2,2'-bipyridyl),[21] in CH_3CN in the absence or presence of Brønsted acids. We also discuss on the controlling factors of the PCET mechanism in C-H oxidation. The manipulation of PCET mechanisms in C-H oxidation by **$Ru^{IV}(O)$** on the basis of proton concentrations provides a good viewpoint to shed light on a boundary region around a mechanistic borderline of PCET mechanisms based on ET properties of **$Ru^{IV}(O)$** including the λ value of PCET. In this paper, we would like to discuss on an oxidative asynchronous CPET mechanism in C-H oxidation by **$Ru^{IV}(O)$** in the presence of Brønsted acids.

RESULTS AND DISCUSSION

Oxidation reactions of BA derivatives by $Ru^{IV}(O)$. An oxidation reaction of benzyl alcohol (BA) showing a one-electron oxidation potential (E_{ox}) of 2.33 V (vs SCE)[22] by **$Ru^{IV}(O)$** was performed in acetonitrile (CH_3CN) at 298 K. The oxidized product of BA was confirmed to be benzaldehyde as the sole two-electron oxidized product (77% yield based on [**$Ru^{IV}(O)$**]) by GC-MS and ^{1}H NMR measurements (Figure 2a; see also Figure S1 and S2 in Supporting Information). In the ^{1}H NMR spectrum, the formation of $[Ru^{II}(MeBPA)(bpy)(NCCD_3)]^{2+}$ ($Ru^{II}(NCCD_3)$) was observed together with the ^{1}H NMR signals derived from benzaldehyde. To elucidate the kinetics of BA oxidation, UV-vis spectral changes were monitored after addition of BA to an CH_3CN solution containing **$Ru^{IV}(O)$** as shown in Figure 2b. The increased absorption band at 434 nm is assigned to that of $Ru^{II}(NCCH_3)$ in comparison with the absorption band of independently prepared $Ru^{II}(NCCH_3)$ (Figure S3). It should be noted that the ligand-exchange reaction from $[Ru^{II}(MeBPA)(bpy)(OH_2)]^{2+}$ to $Ru^{II}(NCCH_3)$ in CH_3CN is relatively slow even in the presence of Brønsted acids (Figure S3).[23] The time profile at 434 nm, which obeyed pseudo-first-order kinetics in the presence of excess BA, was selected for determination of BA oxidation rate. The pseudo-first-order rate constants (k_{obs}) increased linearly with increasing concentrations of BA (Figure 2c). Thus, the second-order rate constant (k_H) was determined to be $(5.7 \pm 0.2) \times 10^{-1}$ M^{-1} s^{-1} from the slope of the linear plot. When BA was replaced by deuterated BA at the benzylic position (BA-d_2), the second-order rate constant (k_D) was determined to be $(2.0 \pm 0.1) \times 10^{-1}$ M^{-1} s^{-1}), which was smaller than k_H, demonstrating a kinetic isotope effect (KIE = k_H/k_D = 2.8). These results indicate that the rate-determining step of BA oxidation by **$Ru^{IV}(O)$** is CPET from BA to **$Ru^{IV}(O)$**.

When we employed 3,4,5-trimethoxybenzyl alcohol ($(MeO)_3$-BA) as a substrate showing a lower oxidation potential (E_{ox} = 1.22 V vs SCE)[22] than that of BA, formation of the corresponding benzaldehyde was confirmed as the sole product in 96% yield based on [**$Ru^{IV}(O)$**], together with the observation of similar UV-vis spectral changes as shown in Figure 3. The second-order rate constants for oxidation reactions of $(MeO)_3$-BA and $(MeO)_3$-BA-d_2 were also determined to be $k_H = 1.4 \pm 0.1$ M^{-1} s^{-1} and $k_D = (6.0 \pm 0.1) \times 10^{-2}$ M^{-1} s^{-1}, showing a large KIE (k_H/k_D = 23). Such a large KIE suggested the involvement of H-tunneling[24] in CPET from $(MeO)_3$-BA to **$Ru^{IV}(O)$**. Similarly, k_H values for other BA derivatives were determined (Figure S4) and listed in Table 1. Judging from these results, oxidation of a series of BA derivatives by **$Ru^{IV}(O)$** proceeded through a CPET mechanism with comparable k_H values in the absence of Brønsted acids. The reason for the fact is that ET oxidation of BA derivatives by **$Ru^{IV}(O)$** is thermodynamically unfavorable in terms of the driving force of ET ($-\Delta G_{et}$) calculated on the basis of

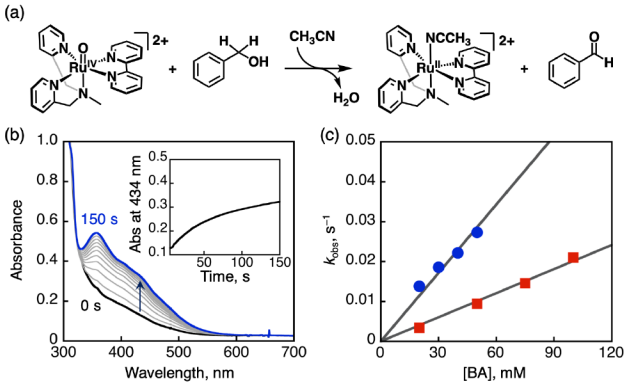

Figure 2. (a) A reaction scheme for BA oxidation by **$Ru^{IV}(O)$**. (b) UV-vis spectral changes at 298 K observed after addition of BA (30 mM) to a CH_3CN solution containing **$Ru^{IV}(O)$** (0.10 mM). Inset: The time profile at 434 nm. (c) Plots of k_{obs} vs [BA] (blue) or [BA-d_2] (red).

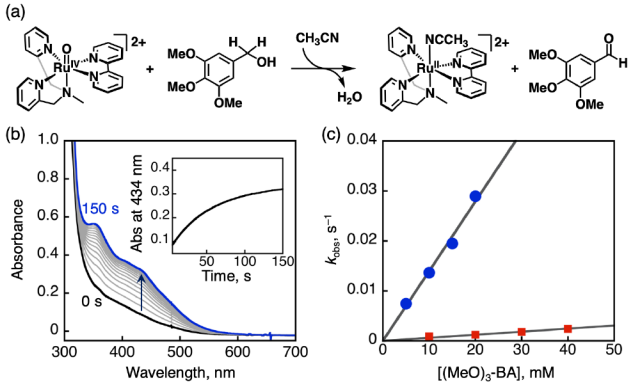

Figure 3. (a) A reaction scheme for $(MeO)_3$-BA oxidation by **$Ru^{IV}(O)$**. (b) UV-vis spectral changes at 298 K observed after addition of $(MeO)_3$-BA (15 mM) to a CH_3CN solution containing **$Ru^{IV}(O)$** (0.10 mM). Inset: The time profile at 434 nm. (c) Plots of k_{obs} vs [$(MeO)_3$-BA] (blue) or [$(MeO)_3$-BA-d_2] (red).

Table 1. One-electron oxidation potentials (E_{ox}) of BA derivatives, driving forces of ET ($-\Delta G_{et}$), and rate constants (k_H, k_D) with KIE values in oxidation of BA derivatives by **Ru^{IV}(O)** in CH_3CN at 298 K

substrate	E_{ox}, V[a]	$-\Delta G_{et}$, eV	k_H, M^{-1} s^{-1}	k_D, M^{-1} s^{-1} (KIE)[b]
BA	2.33	−2.32	(5.7 ± 0.2) × 10^{-1}	(2.0 ± 0.1) × 10^{-1} (KIE = 2.8)
4-Me-BA	2.05	−2.04	(9.0 ± 0.7) × 10^{-1}	n.d.[c]
3,5-$(MeO)_2$-BA	1.49	−1.48	1.2 ± 0.1	n.d.[c]
$(MeO)_3$-BA	1.22	−1.21	1.4 ± 0.1	(6.0 ± 0.1) × 10^{-2} (KIE = 23)
2,5-$(MeO)_2$-BA	1.20	−1.19	1.4 ± 0.1	n.d.[c]

[a] vs SCE [b] KIE values are shown in parentheses [c] not determined

the one-electron reduction potential (E_{red} = 0.01 V vs SCE)[21] of **Ru^{IV}(O)** and E_{ox} of BA derivatives as summarized in Table 1.

Oxidation reactions of BA derivatives by Ru^{IV}(O) in the presence of a Brønsted Acid. In the presence of trifluoroacetic acid (TFA) as a Brønsted acid, the E_{red} values of **Ru^{IV}(O)** exhibited a large positive shift depending on the concentration of TFA.[21] If oxidation of BA derivatives by **Ru^{IV}(O)** is accelerated by the presence of TFA, proton-promoted oxidation is expected to proceed through a transition state bearing enhanced ET-character due to the elevated redox potential of **Ru^{IV}(O)**. According to this hypothesis, we performed oxidation of BA derivatives by **Ru^{IV}(O)** in the presence of TFA. The oxidized products of BA derivatives with TFA were confirmed to be the corresponding benzaldehyde derivatives by GC-MS measurements (69% for BA and 38% for $(MeO)_3$-BA) as shown in Figure S5 in SI. In order to evaluate the effect of TFA on oxidation rates of BA derivatives, second-order rate constants (k_H') of the reactions in the presence of TFA were determined by the same procedure as mentioned above (Figures S6 and S7). In the case of BA oxidation by **Ru^{IV}(O)** in the presence of TFA, we could observe only slight acceleration of k_H' even in the presence of 250 mM TFA (k_H' = (7.7 ± 0.1) × 10^{-1} M^{-1} s^{-1}) in comparison with k_H ((5.7 ± 0.2) × 10^{-1} M^{-1} s^{-1}) in the absence of TFA. Similar k_H' values in BA oxidation with or without TFA indicate no change in PCET mechanisms regardless of E_{red} values of **Ru^{IV}(O)**. In sharp contrast, significant acceleration of $(MeO)_3$-BA oxidation by **Ru^{IV}(O)** was observed in the presence of TFA (2.5 – 550 mM) as shown in Figure 4. The determined k_H' values of $(MeO)_3$-BA were plotted vs [TFA], which showed a first-order relationship in the range of 0 mM < [TFA] < 50 mM and a second-order one above 50 mM of TFA. Such a mixed first- and second-order dependence of k_H' on [TFA] can be given by eq 1,

$$k_H' = k_0' + k_1'[TFA] + k_2'[TFA]^2 \quad (1)$$

where k_0', k_1' and k_2' are the zero-, first-, and second-order rate constants of the $(MeO)_3$-BA oxidation depending on [TFA], respectively. The first- and second-order dependence of k_H' on [TFA] indicates that $(MeO)_3$-BA is oxidized not only by a one-proton-interacted **Ru^{IV}(O)** (**Ru^{IV}(O)**•••H^+) but also by a two-proton-interacted **Ru^{IV}(O)** (**Ru^{IV}(O)**•••$2H^+$) as shown in Scheme 1, whereas the amount of these proton-interacted **Ru^{IV}(O)** species is too small to be spectroscopically detected under the reaction conditions.[25] The individual k_1' and k_2' values were determined to be 240 M^{-2} s^{-1} and 3400 M^{-3} s^{-1}, respectively, by extraction from fitting k_H' vs [TFA] plots. Therefore, the contribution of the term (k_1'[TFA]) in eq 1 to the k_H' value is calculated according to eq 2.

$$\text{contribution of } k_1'[TFA] \text{ to } k_H' \ (\%) = 100 \times k_1'[TFA]/(k_0' + k_1'[TFA] + k_2'[TFA]^2) \quad (2)$$

The contributions of the other fractions, k_0' and k_2'[TFA]^2, were also calculated accordingly. Each fraction (k_0', k_1'[TFA], and k_2'[TFA]^2) obtained was plotted as a function of [TFA] to clarify the range of an intermediate region involving **Ru^{IV}(O)**•••H^+ (0 mM < [TFA] < 50 mM) as shown in Figure 5.

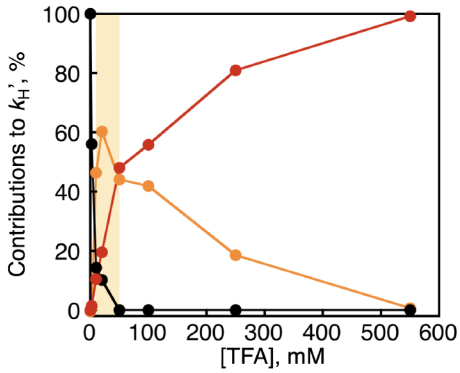

Figure 5. Plots of contribution of each fraction (k_0' (black), k_1'[TFA] (orange), and k_2'[TFA]^2 (red)) to the composite rate constant (k_H') against [TFA].

Scheme 1

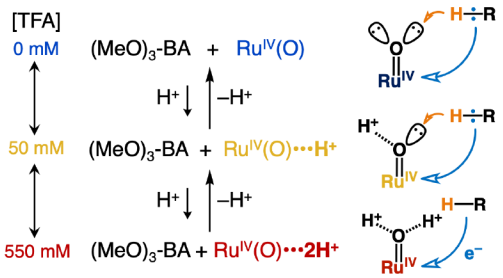

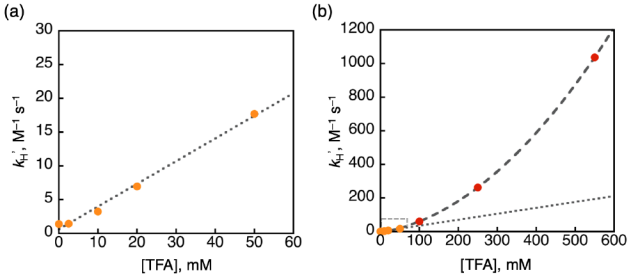

Figure 4. Plots of k_H' vs [TFA] in $(MeO)_3$-BA oxidation by **Ru^{IV}(O)** in the presence of (a) 0-50 mM TFA and (b) 0-550 mM TFA.

In addition, dependence of KIE values of $(MeO)_3$-BA on [TFA] was also investigated in the same range of [TFA] as shown in Figure

S9. At [TFA] = 0 mM, the KIE value (k_H'/k_D'), corresponding to $k_0'(H)/k_0'(D)$, was 23 as mentioned above. The KIE value decreased down to 1.1 ([TFA] = 550 mM) with increasing [TFA], as summarized in Figure 6. According to the procedure mentioned in eq 2, the KIE value for each pathway was determined to be 15 for k_1' and 1.1 for k_2' based on the individual k_1' (240 M^{-2} s^{-1} for $k_1'(H)$ and 36 M^{-2} s^{-1} for $k_1'(D)$) and k_2' values (3400 M^{-3} s^{-1} for $k_2'(H)$ and 3100 M^{-3} s^{-1} for $k_2'(D)$). The obtained KIE value (15) for k_1' of the pathway involving $\mathbf{Ru^{IV}(O)}\cdots H^+$ is larger than KIEs (3.1-8.4, 2.5 mM ≤ [TFA] ≤ 50 mM) determined from k_H' values (eq 1), because the contribution of each fraction (k_0', k_1'[TFA], and k_2'[TFA]^2) depends on [TFA] in the range to the KIE values for k_H'.

The increase of kinetic orders and the decrease of KIE values with increase of [TFA] clearly suggest a sequential change of PCET mechanisms from CPET (KIE = 23) to an intermediate mechanism involving $\mathbf{Ru^{IV}(O)}\cdots H^+$ (KIE = 15), and to stepwise ET/PT (KIE = 1.1) as shown in Figure 6. In other words, the gradual alteration of PCET mechanisms, as reflected on Figure 5, is mainly governed by the enhanced electron-acceptability of $\mathbf{Ru^{IV}(O)}$ due to enhanced interaction with TFA to raise E_{red} values in accordance with increase of [TFA]. The formation of proton-interacted $\mathbf{Ru^{IV}(O)}$ species having one lone pair or none at the oxo ligand ($\mathbf{Ru^{IV}(O)}\cdots H^+$ or $\mathbf{Ru^{IV}(O)}\cdots 2H^+$, respectively) should be related to the alteration of CPET mechanisms and KIE values. As shown in Scheme 1, in the cases of $\mathbf{Ru^{IV}(O)}$ and $\mathbf{Ru^{IV}(O)}\cdots H^+$ that have two and one lone pairs at the oxo ligand, respectively, HAT occurs through CPET involving PT from a C-H bond to a lone pair of the oxo ligand concomitant with ET from the C-H bond to the Ru^{IV} center. In contrast, $\mathbf{Ru^{IV}(O)}$ interacting two protons with the two lone pairs cannot accept a proton from a C-H bond and can only accept an electron from the substrate C-H bond.

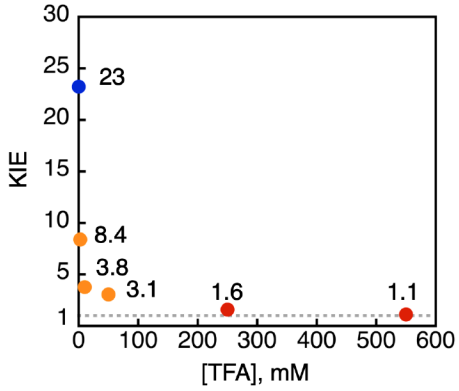

Figure 6. Plots of KIE vs [TFA] in $(MeO)_3$-BA oxidation by $\mathbf{Ru^{IV}(O)}$ in the presence of TFA.

So far, there are several discussions on the alteration of PCET mechanisms in C-H oxidation by $M^{n+}(O)$ complexes, which suggest an borderline between CPET and stepwise ET/PT is nearby $-\Delta G_{et}$ = –0.5 eV.[9,22] According to previous reports, evaluation of the reactivity of $\mathbf{Ru^{IV}(O)}$ in light of the Marcus theory of ET would be indispensable for revealing the alteration of PCET mechanisms. We have already determined the λ value in PCET (λ = 1.26 eV) in PCET reactions from electron donors to $\mathbf{Ru^{IV}(O)}$ in the presence of TFA.[21] It should be noted that the λ value in PCET was almost same in the presence of TFA (2.5, 20, 50, and 250 mM) (Figure S10 in SI). Therefore, $\log k_H$ and $\log k'$ values in oxidation of a series of BA derivatives were plotted against $-\Delta G_{et}$ values that are the driving forces of ET from the substrates to $\mathbf{Ru^{IV}(O)}$ as defined in eq 2. We applied the Marcus equation for adiabatic ET to the analysis as given in eq 3, where k_{et} is defined as a rate constant of ET, k_{diff} as diffusion constant (2.0×10^{10} M^{-1} s^{-1} in CH_3CN), Z as the collision frequency (1×10^{10} M^{-1} s^{-1}), and k_B as the Boltzman constant.

$$-\Delta G_{et} = -e(E_{ox} - E_{red}) \quad (2)$$

$$1/k_{et} = 1/k_{diff} + \{Z\exp[-(\lambda/4)(1 + \Delta G_{et}/\lambda)^2/k_B T]\}^{-1} \quad (3)$$

The $\log k_H$ values for BA derivatives in the absence of TFA are almost the same without dependence on the $-\Delta G_{et}$ values (Figure S10). This indicates that CPET from BA derivatives to $\mathbf{Ru^{IV}(O)}$ should be mainly governed by the BDEs of benzylic C-H bonds of substrates and the $Ru^{III}(OH)$ complex rather than $-\Delta G_{et}$. Although $\log k_H'$ values of BA in the presence of TFA are also intact relative to the $-\Delta G_{et}$ values, the plots of $\log k_n'[TFA]^n$ (n = 0,1,2) of $(MeO)_3$-BA are converging on the Marcus parabola of PCET reactions from electron donors to $\mathbf{Ru^{IV}(O)}$ with TFA (λ = 1.26 eV[21]) as shown in Figure 7. These results strongly suggest that the PCET mechanism in $(MeO)_3$-BA oxidation is switched from CPET to stepwise ET/PT as discussed before. The borderline of PCET mechanisms was estimated to be in the range of the boundary region involving $\mathbf{Ru^{IV}(O)}\cdots H^+$ as illustrated in orange color in Figure 7, which is the same range in Figure 5 (0 mM < [TFA] < 50 mM). Therefore, this result indicates the $\mathbf{Ru^{IV}(O)}\cdots H^+$ species correlates with the appearance of a different mechanism of PCET in the region. Although the borderline of PCET mechanisms between CPET and stepwise ET/PT by $M^{n+}(O)$ complexes has been reported to be in the range of –0.5 eV < $-\Delta G_{et}$ < –0.3 eV,[9,22] our result suggests another mechanism in the boundary region involving a proton-interacted high-valent $M^{n+}(O)$ complex, probably an oxidative asynchronous CPET.

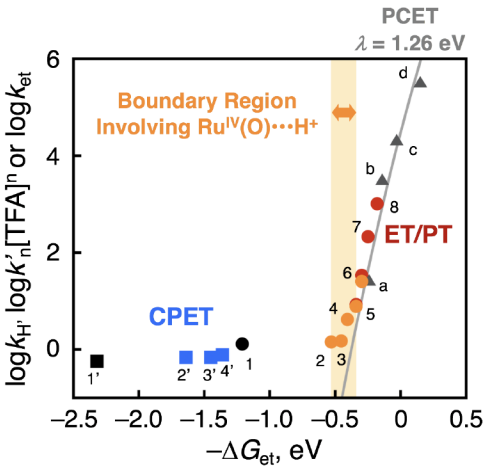

Figure 7. Plots of $\log k_H'$, $\log(k_n'[TFA]^n)$ (n = 0,1,2), or $\log k_{et}$ against driving forces of ET ($-\Delta G_{et}$). The filled circles show the $\log k_n'[TFA]^n$ of the oxidation reaction of $(MeO)_3$-BA in CH_3CN at 298 K in various concentrations of TFA. The numbers of data points (1 – 8) correspond to those listed in Table 2. The squares show $\log k_H'$ of the oxidation reaction of BA in CH_3CN at 298 K in various concentrations of TFA [(1') TFA 0 mM, (2') 2.5 mM, (3') 50 mM, (4') 250 mM]. The triangles represent the $\log k_{et}$ values of the ET reactions from electron donors to $\mathbf{Ru^{IV}(O)}$ in CH_3CN at 243 K in the presence of TFA (2.5 mM) [(a) $(MeO)_3$-Ph, (b) Ph_3N, (c) Br_2Fc, (d) BrFc]. The grey line is the Marcus parabola with λ = 1.26 eV obtained for PCET reactions from various electron donors to $\mathbf{Ru^{IV}(O)}$ in CH_3CN.[21]

Table 2. One-electron oxidation potentials (E_{red}) of **Ru^{IV}(O)**, $-\Delta G_{et}$, logk_n'[TFA]^n (n = 1,2) in $(MeO)_3$-BA oxidation by **Ru^{IV}(O)**

no.	[TFA], mM	E_{red}, V[a]	$-\Delta G_{et}$, eV	logk_1'[TFA]	logk_2'[TFA]^2
1	0	0.01	−1.21	-	-
2	2.5	0.69	−0.53	0.16	-
3	10	0.82	−0.40	0.18	-
4	20	0.85	−0.37	0.62	-
5	50	0.89	−0.33	0.89	0.93
6	100	0.94	−0.28	1.4	1.5
7	250	0.99	−0.23	-	2.3
8	550	1.04	−0.18	-	3.0

[a] E_{red} values of **Ru^{IV}(O)** (V vs SCE)

In order to clarify the borderlines of sequential alteration of PCET mechanisms as shown in Scheme 1, dependence of activation parameters on [TFA] in both BA and $(MeO)_3$-BA oxidation by **Ru^{IV}(O)** was scrutinized at several temperatures (Figures S11 and S12). Although there is no difference in BA oxidation with or without TFA, Eyring plots of k_H' for $(MeO)_3$-BA oxidation are clearly depending on [TFA] as shown in Figure S12. In order to evaluate activation parameters ($\Delta H^{\ddagger}$, $\Delta S^{\ddagger}$ and $\Delta G^{\ddagger}$) for individual k_n' (n = 0,1,2) values, extractions of k_n' at each [TFA] were performed on the basis of the Eyring plot and contribution of each fraction to k_H' (Figure S13 and eqs s1-4). In the absence of TFA (k_H' = k_0'; eq s2 in the SI), $\Delta H^{\ddagger}$ and $\Delta S^{\ddagger}$ values in $(MeO)_3$-BA oxidation were determined to be 5.1 kcal mol^{-1} and −41 cal mol^{-1} K^{-1}, which are comparable with those of bimolecular oxidation reactions by a reported **Ru^{IV}(O)** complex via CPET.[15a] In the presence of 550 mM TFA (k_H' = k_2'[TFA]^2; eq s4 in the SI), the $\Delta H^{\ddagger}$ and $\Delta S^{\ddagger}$ values for k_2' were determined to be 5.4 kcal mol^{-1} and −25 cal mol^{-1} K^{-1}, respectively, on the basis of the Eyring plot (Figure S13) with approximation according to eq s4 in the SI. Finally, according to eq s3 in the SI, we calculated the k_1' values in the range of 10 mM ≤ [TFA] ≤ 50 mM on the basis of the contribution of the fraction (k_1'[TFA]) to k_H' as shown in Figure 5. Using the k_1' values obtained, an Eyring plot was provided as shown in Figure 8 (orange line). The $\Delta H^{\ddagger}$ and $\Delta S^{\ddagger}$ values for k_1' were obtained from the Eyring plot (Figure 8), affording the activation parameters, $\Delta H^{\ddagger}$ = 3.4 ± 0.2 kcal mol^{-1}, $\Delta S^{\ddagger}$ = −37 ± 2 cal mol^{-1} K^{-1}, and $\Delta G^{\ddagger}$ = 14 ± 1 kcal mol^{-1} at 298 K, respectively. The Eyring plot for k_1' is shown in Figure 8 together with those for k_0' and k_2'; the plot for k_1' lies in between the two lines with a smaller slope. The activation parameters obtained for k_n' (n = 0,1,2) are listed in Table 3, in which the smallest $\Delta H^{\ddagger}$ value for k_1' could be a critical factor to suggest the existence of another mechanism in the boundary region involving **Ru^{IV}(O)•••**H$^+$ rather than the admixture of the CPET and ET/PT mechanisms as two extremes.

In the range of 0 mM < [TFA] ≤ 50 mM, the decrease of $\Delta H^{\ddagger}$ values contribute to lowering the $\Delta G^{\ddagger}$ values to accelerate the $(MeO)_3$-BA oxidation by **Ru^{IV}(O)•••H$^+$** with a first-order dependence of k_H' on [TFA] and smaller KIE values. In contrast, in the range of [TFA] ≥ 50 mM, the increase of $\Delta S^{\ddagger}$ values should cause the decrease of $\Delta G^{\ddagger}$ values to enhance the $(MeO)_3$-BA oxidation by **Ru^{IV}(O)•••2H$^+$** despite the increase of $\Delta H^{\ddagger}$. The two-step change of activation parameters depending on [TFA] can be attributed to the involvement of **Ru^{IV}(O)•••**H$^+$ in the range of 0 mM < [TFA] ≤ 50 mM and **Ru^{IV}(O)•••**2H$^+$ in the range of [TFA] ≥ 50 mM, as the main reactive species, as depicted in Scheme 2. Therefore, the switching of activation parameters depending on [TFA] clearly indicate that the PCET mechanisms alter around [TFA] = 50 mM from CPET to a boundary region involving one-proton-interacted **Ru^{IV}(O)•••**H$^+$, and to ET/PT involving **Ru^{IV}(O)•••**2H$^+$. In the boundary region, the reaction is assumed to proceed *via* oxidative asynchronous CPET as shown in Figure 1, as suggested by the kinetic analysis.

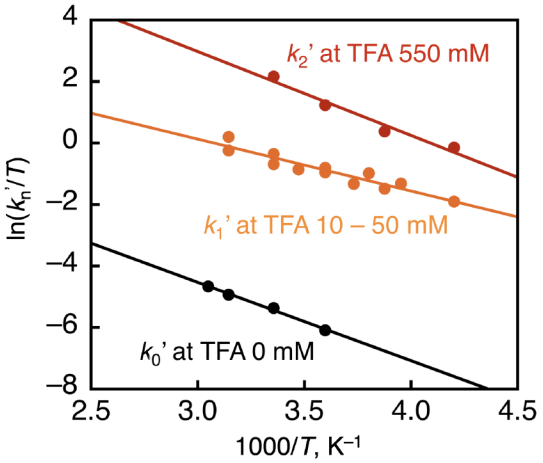

Figure 8. Eyring plots of k_n' (n = 0,1,2) in eq 1 for the oxidation of $(MeO)_3$-BA by **Ru^{IV}(O)** at various temperatures in CH_3CN.

Table 3. Individual activation parameters ($\Delta H^{\ddagger}$, $\Delta S^{\ddagger}$, and $\Delta G^{\ddagger}$) determined for each rate constant k_n' (n = 0,1,2) in $(MeO)_3$-BA oxidation by **Ru^{IV}(O)** in the presence of TFA

rate constant	$\Delta H^{\ddagger}$, kcal mol^{-1}	$\Delta S^{\ddagger}$, cal mol^{-1} K^{-1}	$\Delta G^{\ddagger}$[a], kcal mol^{-1}
k_0'	5.1	−41	17
k_1'	3.4 ± 0.2	−37 ± 2	14 ± 1
k_2'	5.4	−25	13

[a] at 298 K

Scheme 2

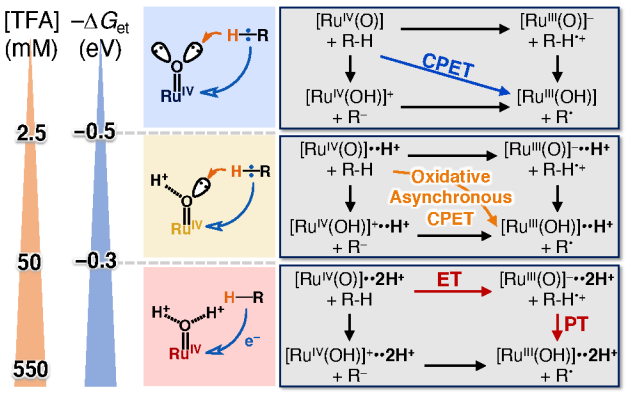

Insight into the Transition States of CPET in the Presence of TFA on the Basis of DFT Calculations.

In order to lend credence to the involvement of the **$Ru^{IV}(O)\cdots H^+$** species in the putative oxidative asynchronous CPET, we performed DFT calculations to analyze the potential energy surface along the reaction coordinate by changing an interatomic distance between a benzylic hydrogen atom of $(MeO)_3$-BA and the oxo ligand of **$Ru^{IV}(O)\cdots H^+$** in CPET from $(MeO)_3$-BA to **$Ru^{IV}(O)\cdots H^+$**. As described in the experimental section, we examined two models by fixing the position of H^+ of TFA for understanding the HAT mechanism. When the position of H^+ was fixed at 1.05 Å from the O_{TFA} atom of the carboxyl group of TFA (Figure 9A), the oxidation state of **$Ru^{IV}(O)$** was intact. Under this condition, change of atomic distance between the benzylic hydrogen and the oxo ligand afforded a potential surface as a blue trace in Figure 9C. On the other hand, the position of H^+ was fixed nearby the oxo moiety of **$Ru^{IV}(O)$** to be **$Ru^{IV}(O)\cdots H^+$** at 1.04 Å resulted in stabilization of $Ru^{III}(OH)$ and $(MeO)_3$-$BA^{\bullet+}$, involving a product of ET from $(MeO)_3$-BA to **$Ru^{IV}(O)\cdots H^+$** (Figure 9B). In this case, change of atomic distance between the benzylic hydrogen and the oxo ligand afforded a potential surface as a red trace in Figure 9C. As can be seen in Figure 9C, in the range of 1.2 – 1.55 Å of the (C-)H•••O(-Ru) distance, the potential surface of the ET-product state (red trace) lies below that of **$Ru^{IV}(O)\cdots H^+$** (blue trace). Thus, in the range of the (C-)H•••O(-Ru) distance, the ET products are more favored than the **$Ru^{IV}(O)\cdots$**H(TFA) and $(MeO)_3$-BA; in other words, the access of the substrate to the **$Ru^{IV}(O)$** moiety induces ET from the substrate to the $Ru^{IV}(O)\cdots H^+$(TFA). This result indicates that, under the conditions, oxidative asynchronous CPET is considered to be a preferable reaction pathway in terms of the lower activation barrier. Therefore, we concluded that **$Ru^{IV}(O)\cdots H^+$** species is capable of oxidizing $(MeO)_3$-BA via oxidative asynchronous CPET in the boundary region involving **$Ru^{IV}(O)\cdots H^+$**.

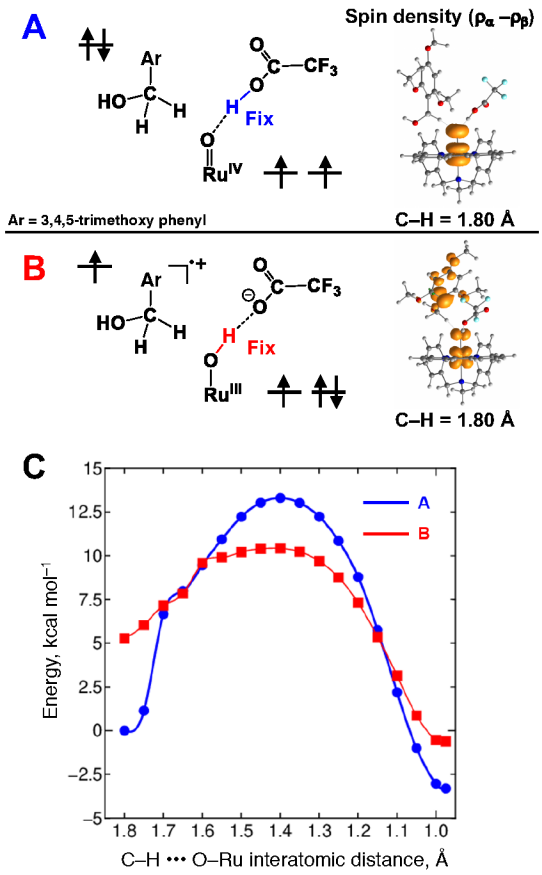

Figure 9. DFT calculations for two models by fixing the position of H^+ ((A) the position of H^+ was fixed at 1.05 Å from the O-atom of TFA, (B) the position of H^+ was fixed at 1.04 Å from the oxo moiety of **$Ru^{IV}(O)$**). (C) The potential energy surfaces along the reaction coordinate of the two models.

CONCLUSION

In this work, we have discussed the PCET mechanisms in oxidation of benzyl alcohol derivatives by an isolated **$Ru^{IV}(O)$** complex in the absence or presence of TFA as a proton source. The reaction mechanism was scrutinized on the basis of kinetic analysis and elucidated in light of Marcus theory of ET to reveal the borderline of alteration of PCET mechanisms from CPET to stepwise ET/PT. The Marcus plot shows a clear crossing point involving **$Ru^{IV}(O)\cdots H^+$** between CPET and ET/PT, which is a general aspect for alteration of PCET mechanisms in the range of -0.5 eV $< -\Delta G_{et} < -0.3$ eV by several metal-oxo species.[9, 22] The kinetic analyses are suggestive of another CPET mechanism, probably an oxidative asynchronous CPET, involving **$Ru^{IV}(O)\cdots H^+$** as a reactive species in the boundary region of proton concentration mentioned above. As presented in this work, a mechanistic insight into PCET reactions depending on concentrations of Brønsted acids will provide a new avenue for novel reactivity of a transition-metal-oxo complex in substrate oxidation toward selective oxidation of substrates bearing lower oxidation potentials.

ASSOCIATED CONTENT

Supporting Information

The Supporting Information is available free of charge on the ACS Publications website. Experimental details and analytical data, including Figures S1-S13 (PDF)

AUTHOR INFORMATION

Corresponding Author

kojima@chem.tsukuba.ac.jp

ACKNOWLEDGMENT

This work was supported by Grants-in-Aid (Nos. 17H03027, and 17K14456) from the Japan Society of Promotion of Science (JSPS, MEXT) of Japan and the Cooperative Research Program of "Network Joint Research Center for Materials and Devices" (JPMXS0422300120). Financial supports through CREST (JST) are also appreciated (JPMJCR16P1 and JPMJCR15P5).

REFERENCES

(1) (a) Que, L., Jr.; Ho, R. Y. N. Dioxygen Activation by Enzymes with Mononuclear Non-Heme Iron Active Sites. *Chem. Rev.* **1996**, *96*, 2607-2624. (b) Krebs, C.; Galonić Fujimori, D.; Walsh, C. T.; Bollinger, J. M. Non-Heme Fe(IV)–Oxo Intermediates. *Acc. Chem. Res.* **2007**, *40*, 484-492. (c) Galonić, D. P.; Barr, E. W.; Walsh, C. T.; Bollinger, J. M., Jr; Krebs, C. Two Interconverting Fe(IV) Intermediates in Aliphatic Chlorination by the Halogenase CytC3. *Nat. Chem. Biol.* **2007**, *3*, 113-116.

(2) (a) Nam, W. High-Valent Iron(IV)-Oxo Complexes of Heme and Non-Heme Ligands in Oxygenation Reactions. *Acc. Chem. Res.* **2007**, *40*, 522-531. (b) Que, L. The Road to Non-Heme Oxoferryls and Beyond. *Acc. Chem. Res.* **2007**, *40*, 493-500. (c) Goldberg, D. P. Corrolazines: New Frontiers in High-Valent Metalloporphyrinoid Stability and Reactivity. *Acc. Chem. Res.* **2007**, *40*, 626–634.

(3) (a) Borovik, A. S. Role of Metal–oxo Complexes in the Cleavage of C–H Bonds. *Chem. Soc. Rev.* **2011**, *40*, 1870-1874. (b) Lam, W. W. Y.; Man, W.-L.;Lau, T.-C. Mechanisms of Oxidation by Trans-dioxoruthenium(VI) Complexes Containing Macrocyclic Tertiary Amine Ligands. *Coord. Chem. Rev.* **2007**, *251*, 2238-2252.

(4) Xue, X.-S.; Ji, P.; Zhou, B.; Cheng, J.-P. The Essential Role of Bond Energetics in C–H Activation/Functionalization. *Chem. Rev.* **2017**, *117*, 8622-8648.

(5) (a) Mayer, J. M. Hydrogen Atom Abstraction by Metal-Oxo Complexes: Understanding the Analogy with Organic Radical Reactions. *Acc. Chem. Res.* **1998**, *31*, 441-450. (b) Mayer, J. M. Understanding Hydrogen Atom Transfer: From Bond Strengths to Marcus Theory. *Acc. Chem. Res.* **2011**, *44*, 36-46. (c) Nam, W.; Lee, Y.-M.; Fukuzumi, S. Tuning Reactivity and Mechanism in Oxidation Reactions by Mononuclear Nonheme Iron(IV)-Oxo Complexes. *Acc. Chem. Res.* **2014**, *47*, 1146-1154.

(6) (a) Mayer, J. M. Proton-Coupled Electron Transfer: A Reaction Chemist's View. *Annu. Rev. Phys. Chem.* **2004**, *55*, 363-390. (b) Warren, J. J.; Tronic, T. A.; Mayer, J. M. Thermochemistry of Proton-Coupled Electron Transfer Reagents and Its Implications. *Chem. Rev.* **2010**, *110*, 6961-7001.

(7) (a) Huynh, M. H. V.; Meyer, T. J. Proton-Coupled Electron Transfer. *Chem. Rev.* **2007**, *107*, 5004-5064. (b) Weinberg, D. R.; Gagliardi, C. J.; Hull, J. F.; Murphy, C. F.; Kent, C. A.; Westlake, B. C.; Paul, A.; Ess, D. H.; McCafferty, D. G.; Meyer, T. J. Proton-Coupled Electron Transfer. *Chem. Rev.* **2012**, *112*, 4016-4093.

(8) (a) Hammes-Schiffer, S. Theory of Proton-Coupled Electron Transfer in Energy Conversion Processes. *Acc. Chem. Res.* **2009**, *42*, 1881-1889. (b) Hammes-Schiffer, S.; Stuchebrukhov, A. A. Theory of Coupled Electron and Proton Transfer Reactions. *Chem. Rev.* **2010**, *110*, 6939-6960.

(9) (a) Fukuzumi, S. Electron-Transfer Properties of High-Valent Metal-Oxo Complexes. *Coord. Chem. Rev.* **2013**, *257*, 1564-1575. (b) Park, J.; Morimoto, Y.; Lee, Y.-M.; Nam, W.; Fukuzumi, S. Proton-Promoted Oxygen Atom Transfer vs Proton-Coupled Electron Transfer of a Non-Heme Iron(IV)-Oxo Complex. *J. Am. Chem. Soc.* **2012**, *134*, 3903-3911. (c) Park, J.; Lee, Y.-M.; Nam, W.; Fukuzumi, S. Brønsted Acid-Promoted C–H Bond Cleavage via Electron Transfer from Toluene Derivatives to a Protonated Nonheme Iron(IV)-Oxo Complex with No Kinetic Isotope Effect. *J. Am. Chem. Soc.* **2013**, *135*, 5052-5061. (d) Yoon, H.; Lee, Y.-M.; Wu, X.; Cho, K.-B.; Sarangi, R.; Nam, W.; Fukuzumi, S. Enhanced Electron-Transfer Reactivity of Nonheme Manganese(IV)–Oxo Complexes by Binding Scandium Ions. *J. Am. Chem. Soc.* **2013**, *135*, 9186-9194. (e) Chen, J.; Yoon, H.; Lee, Y.-M.; Seo, M. S.; Sarangi, R.; Fukuzumi, S.; Nam, W. Tuning the Reactivity of Mononuclear Nonheme Manganese(IV)-Oxo Complexes by Triflic Acid. *Chem. Sci.* **2015**, *6*, 3624-3632. (f) Morimoto, Y.; Park, J.; Suenobu, T.; Lee, Y.-M.; Nam, W.; Fukuzumi, S. Mechanistic Borderline of One-Step Hydrogen Atom Transfer versus Stepwise Sc^{3+}-Coupled Electron Transfer from Benzyl Alcohol Derivatives to a Non-Heme Iron(IV)-Oxo Complex. *Inorg. Chem.* **2012**, *51*, 10025-10036. (g) Park, J.; Morimoto, Y.; Lee, Y.-M.; Nam, W.; Fukuzumi, S. Unified View of Oxidative C-H Bond Cleavage and Sulfoxidation by a Nonheme Iron(IV)-Oxo Complex via Lewis Acid-Promoted Electron Transfer. *Inorg. Chem.* **2014**, *53*, 3618-3628.

(10) Goetz, M. K.; Anderson, J. S. Experimental Evidence for pK_a-Driven Asynchronicity in C–H Activation by a Terminal Co(III)-Oxo Complex. *J. Am. Chem. Soc.* **2019**, *141*, 4051-4062.

(11) (a) Usharani, D.; Lacy, D. C.; Borovik, A. S.; Shaik, S. Dichotomous Hydrogen Atom Transfer vs Proton-Coupled Electron Transfer During Activation of X–H Bonds (X = C, N, O) by Nonheme Iron-Oxo Complexes of Variable Basicity. *J. Am. Chem. Soc.* **2013**, *135*, 17090-17104.(b) Bím, D.; Maldonado-Domínguez, M.; Rulíšek, L.; Srnec, M. Beyond the Classical Thermodynamic Contributions to Hydrogen Atom Abstraction Reactivity. *Proc. Natl. Acad. Sci. U. S. A.* **2018**, *115*, E10287-E10294.

(12) Mandal, M.; Elwell, C. E.; Bouchey, C. J.; Zerk, T. J.; Tolman, W. B.; Cramer, C. J. Mechanisms for Hydrogen-Atom Abstraction by Mononuclear Copper(III) Cores: Hydrogen-Atom Transfer or Concerted Proton-Coupled Electron Transfer? *J. Am. Chem. Soc.* **2019**, *141*, 17236-17244.

(13) Darcy, J. W.; Kolmar, S. S.; Mayer, J. M. Transition State Asymmetry in C–H Bond Cleavage by Proton-Coupled Electron Transfer. *J. Am. Chem. Soc.* **2019**, *141*, 10777-10787.

(14) (a) Fenwick, C. W.; English, A. M.; Wishart, J. F. pH and Driving Force Dependence of Intramolecular Oxyferryl Heme Reduction in Myoglobin. *J. Am. Chem. Soc.* **1997**, *119*, 4758-4764. (b) Comba, P.; Fukuzumi, S.; Koke, C.; Martin, B.; Löhr, A.-M.; Straub, J. A Bispidine Iron(IV)-Oxo Complex in the Entatic State. *Angew. Chem., Int. Ed.* **2016**, *55*, 11129-11133. (c) Bataineh, H.; Pestovsky, O.; Bakac, A. Electron Transfer Reactivity of the Aqueous Iron(IV)-Oxo Complex. Outer-Sphere vs Proton-Coupled Electron Transfer. *Inorg. Chem.* **2016**, *55*, 6719-6724.

(15) (a) Bryant, J. R.; Mayer, J. M. Oxidation of C−H Bonds by $[(bpy)_2(py)Ru^{IV}O]^{2+}$ Occurs by Hydrogen Atom Abstraction. *J. Am. Chem. Soc.* **2003**, *125*, 10351-10361. (b) Bryant, J. R.; Matsuo, T.; Mayer, J. M. Cumene Oxidation by cis-$[Ru^{IV}(bpy)_2(py)(O)]^{2+}$, Revisited. *Inorg. Chem.* **2004**, *43*, 1587-1592. (c) Waidmann, C. R.; Zhou, X.; Tsai, E. A.; Kaminsky, W.; Hrovat, D. A.; Borden, W. T.; Mayer, J. M. Slow Hydrogen Atom Transfer Reactions of Oxo- and Hydroxo-Vanadium Compounds: The Importance of Intrinsic Barriers. *J. Am. Chem. Soc.* **2009**, *131*, 4729-4743.

(16) Mitome, H.; Ishizuka, T.; Kotani, H.; Shiota, Y.; Yoshizawa, K.; Kojima, T. Mechanistic Insights into C–H Oxidations by Ruthenium(III)-Pterin Complexes: Impact of Basicity of the Pterin Ligand and Electron Acceptability of the Metal Center on the Transition States. *J. Am. Chem. Soc.* **2016**, *138*, 9508-9520.

(17) Che, C. M.; Yam, V. W. W.; Mak, T. C. W. A Novel Monooxoruthenium(V) Complex Containing a Polydentate Pyridyl Amine Ligand. Syntheses, Reactivities, and X-Ray Crystal Structure of $[Ru^{III}(N_4O)(H_2O)](ClO_4)_2$. *J. Am. Chem. Soc.* **1990**, *112*, 2284-2291.

(18) (a) Moyer, B. A.; Thompson, M. S.; Meyer, T. J. Chemically Catalyzed Net Electrochemical Oxidation of Alcohols, Aldehydes, and Unsaturated Hydrocarbons Using the System $(trpy)(bpy)Ru(OH_2)^{2+}/(trpy)(bpy)RuO^{2+}$. *J. Am. Chem. Soc.* **1980**, *102*, 2310-2312. (b) Moyer, B. A.; Meyer, T. J. Properties of the Oxo/Aqua System $(bpy)_2(py)RuO^{2+}/(bpy)_2(py)Ru(OH_2)^{2+}$. *Inorg. Chem.* **1981**, *20*, 436-444. (c) Gilbert, J.; Roecker, L.; Meyer, T. J. Hydrogen Atom Transfer in the Oxidation of Hydrogen Peroxide by $[(bpy)_2(py)Ru^{IV}O]^{2+}$ and by $[(bpy)_2(py)Ru^{III}OH]^{2+}$. *Inorg. Chem.* **1987**, *26*, 1126-1132. (d) Concepcion, J. J.; Jurss, J. W.; Templeton, J. L.; Meyer, T. J. Mediator-Assisted Water Oxidation by the Ruthenium "blue Dimer" cis,cis-$[(bpy)_2(H_2O)RuORu(OH_2)(bpy)_2]^{4+}$. *Proc. Natl. Acad. Sci. U.S.A.* **2008**, *105*, 17632-17635.

(19) (a) Groves, J. T.; Quinn, R. Models of Oxidized Heme Proteins. Preparation and Characterization of a Trans-dioxoruthenium(VI) Porphyrin Complex. *Inorg. Chem.* **1984**, *23*, 3844-3846. (b) Groves, J. T.; Quinn, R. Aerobic Epoxidation of Olefins with Ruthenium Porphyrin Catalysts. *J. Am. Chem. Soc.* **1985**, *107*, 5790-5792. (c) Boaz, N. C.; Bell, S. R.; Groves, J. T. Ferryl Protonation in Oxoiron(IV) Porphyrins and Its Role in Oxygen Transfer. *J. Am. Chem. Soc.* **2015**, *137*, 2875-2885.

(20) (a) Hirai, Y.; Kojima, T.; Mizutani, Y.; Shiota, Y.; Yoshizawa, K.; Fukuzumi, S. Ruthenium-Catalyzed Selective and Efficient Oxygenation of Hydrocarbons with Water as an Oxygen Source. *Angew. Chem., Int. Ed.* **2008**, *47*, 5772 - 5776. (b) Kojima, T.; Nakayama, K.; Ikemura, K.; Ogura, T.; Fukuzumi, S. Formation of a Ruthenium(IV)-Oxo Complex by Electron-Transfer Oxidation of a Coordinatively Saturated Ruthenium(II) Complex and Detection of Oxygen-Rebound Intermediates in C–H Bond Oxygenation. *J. Am. Chem. Soc.* **2011**, *133*, 11692-11700. (c) Ishizuka, T.; Kotani, H.; Kojima, T. Characteristics and Reactivity of Ruthenium–oxo Complexes. *Dalton Trans.* **2016**, *45*, 16727-16750.

(21) Kotani, H.; Shimomura, H.; Horimoto, M.; Ishizuka, T.; Shiota, Y.; Yoshizawa, K.; Yanagisawa, S.; Kawahara-Nakagawa, Y.; Kubo, M.; Kojima, T. Fundamental Electron-Transfer and Proton-Coupled Electron-Transfer Properties of Ru(IV)-Oxo Complexes. *Dalton Trans.* **2019**, *48*, 13154-13161.

(22) Kotani, H.; Kaida, S.; Ishizuka, T.; Sakaguchi, M.; Ogura, T.; Shiota, Y.; Yoshizawa, K.; Kojima, T. Formation and Characterization of a Reactive Chromium(V)–oxo Complex: Mechanistic Insight into Hydrogen-Atom Transfer Reactions. *Chem. Sci.* **2015**, *6*, 945-955.

(23) Rapaport, I.; Helm, L.; Merbach, A. E.; Bernhard, P.; Ludi, A. High-Pressure NMR Kinetics. Part 34. Variable-Temperature and Variable-Pressure NMR Kinetic Study of Solvent Exchange on hexaaquaruthenium(3+) and -(2+) and hexakis(acetonitrile)ruthenium(2+). *Inorg. Chem.* **1988**, *27*, 873-879.

(24) (a) Kohen, A.; Klinman, J. P. Enzyme Catalysis: Beyond Classical Paradigms. *Acc. Chem. Res.* **1998**, *31*, 397-404. (b) Layfield, J. P.; Hammes-Schiffer, S. Hydrogen Tunneling in Enzymes and Biomimetic Models. *Chem. Rev.* **2013**, *114*, 3466-3494. (c) Cong, Z.; Kinemuchi, H.; Kurahashi, T.; Fujii, H. Factors Affecting Hydrogen-Tunneling Contribution in Hydroxylation Reactions Promoted by Oxoiron(IV) Porphyrin π-Cation Radical Complexes. *Inorg. Chem.* **2014**, *53*, 10632 - 10641.

(25) No apparent spectroscopic change was observed to indicate the formation of proton-interacted $\mathbf{Ru^{IV}(O)}$ even in the excess amount of TFA (Figure S8). See also ref. 9b, c.

TOC

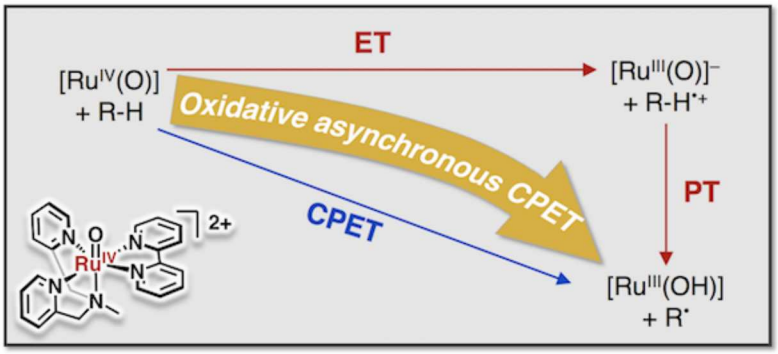
ET
[Ru^IV(O)]
+ R-H
[Ru^III(O)]^−
+ R-H^•+
Oxidative asynchronous CPET
CPET
PT
[Ru^III(OH)]
+ R^•
2+
Ru^IV
O
N